Indian J Phys (January 2018) 92(1):97–109
https://doi.org/10.1007/s12648-017-1069-0

ORIGINAL PAPER

Microstructure and spectroscopic investigations of calcium zinc bismuth phosphate glass ceramics doped with manganese ions

A Suneel Kumar, M V Sambasiva Rao, G Chinna Ram and D Krishna Rao*

Department of Physics, Acharya Nagarjuna University, Nagarjuna Nagar, AP 522510, India

Received: 25 February 2017 / Accepted: 23 May 2017 / Published online: 13 July 2017

Abstract: Multi-component $10CaF_2$–$20ZnO$–$(15 - x)Bi_2O_3$–$55P_2O_5$:$xMnO$ ($0 \leq x \leq 2.5$) glass ceramics were synthesised by melt quenching technique and heat treatment. The prepared glass ceramics were characterised by XRD, DTA, EDS and SEM. Spectroscopic studies such as optical absorption, EPR, FTIR and Raman were also carried out on these glass ceramics. The XRD and SEM studies have indicated that ceramic samples contain well defined and randomly distributed grains of different crystalline phases. The observed increase of enthalpy from DTA patterns up to 1 mol% of MnO indicates that the crystallisation starts initially from the surface of the material then gradually it is extended to the volume of the material and this influence is meagre at higher concentrations of MnO. The absorption spectra of manganese doped glass ceramics have exhibited two types of conventional bands; one due to Mn^{2+} ions and other due to Mn^{3+} ions. The EPR spectra of MnO doped glass ceramics showed a resonance signal around $g_2 = 2.023$ with a six line hyperfine structure and another signal at about $g_1 = 4.314$. The relative intensity and half-width of these two signals are observed to increase with the increase in the concentration of manganese ions up to 1 mol% beyond this concentration it is found to decrease. Such observation indicates the conversion of part of Mn^{2+} ions into Mn^{3+} ions in the glass ceramic matrix. The observed increase in the intensity of symmetrical structural units at the expense of asymmetrical structural units from the FTIR and Raman spectra at higher concentration of MnO indicating that Mn^{2+} ions occupy the network forming positions in the glass ceramic structure.

Keywords: Calcium zinc bismuth phosphate glass ceramics; EPR; Crystallization; Raman and optical spectroscopy; Delocalization process; Insulators; SEM; X-ray diffraction; Infrared spectra

PACS Nos.: 87.64.kh; 87.15.nt; 81.05.Je; 74.25.nd; 73.20.Jc; 72.80.Sk; 68.37.Hk; 66.30.hh; 33.20.Ea

1. Introduction

Glass ceramic materials have one or more crystalline phases in a form of small crystals are produced in glass body during thermal treatment. They have good useful properties for mechanical, electrical, thermal and active as well as passive optical applications. They contain high chemical durability with no crack growth inside and retain transparency. Now-a-days transparent glass ceramics attracted a marked up attention of researchers and manufacturers. Transparent glass ceramics have been used in the field of laser technology due to their lower production costs relative to crystals and in up conversion devices etc., when doped with transition metal ions or rare-earth ions [1, 2].

The objective of latest interest on phosphate based glasses and glass ceramics is owing to their precious physical and spectroscopic properties. Because of low thermo-optical coefficient and large emission, they are suitable materials for high power lasers. The majority of bioactive materials have been prepared based on these glasses [3, 4]. The chemical durability of phosphate glass ceramic system is greatly improved by properly adding one or more oxides such as ZnO, Bi_2O_3 and alkali earth fluoride CaF_2 etc., [5, 6]. Besides these phosphate glasses mixed with heavy metal oxide Bi_2O_3 have wide and potential applications in the field of optical glasses with high refractive indices, low melting temperature, semiconducting glasses and also as a shielding candidate for gamma irradiation [7].

*Corresponding author, E-mail: krdhanekula@yahoo.co.in

Among various glass ceramics, zinc bismuth phosphate glass ceramics are being broadly used in solid state batteries, energy storage devices, laser hosts and as fast ion conducting materials [8]. Calcium phosphate glass ceramics may be adapted to be used as a drug delivery carrier or as cavity filler for maxillofacial surgery, among other applications [9].

In recent years, transition metal ions have been used to investigate the glass structure because of their outer d-electron orbital functions have a wide radial distribution. Among the various transition metal ions, manganese ion is particularly an interesting ion and is extensively investigated in various glasses and glass ceramics since it exhibits different valence states from +2 to +7[(Mn^{2+} ($3d^5$), Mn^{3+} ($3d^4$), Mn^{4+} ($3d^3$), Mn^{5+} ($3d^2$), Mn^{6+} ($3d^1$) and Mn^{7+} ($3d^0$)] depends upon the quantitative properties of modifiers and glass formers, size of the ions in the glass structure, mobility of the modifier cation and strength of field. The ions Mn^{2+} and Mn^{4+} act as luminescent activators while Mn^{3+} and Mn^{2+} ions are well-known paramagnetic ions. Mn^{2+} ions participate in the glass network in octahedral (six-coordinated) and tetrahedral (four-coordinated) structural units having small magnetic anisotropy due to zero orbital angular momentum where as Mn^{3+} ions occupy mainly octahedral (six-coordinated) structural units having large magnetic anisotropy because of their strong spin–orbit interaction of the 3d orbitals [5, 10]. The MnO_4 units alternate with BO_4 and PO_4 units, whereas octahedral Mn ions act as modifiers and induce structural defects. Further these borophosphate glasses doped with manganese ions do exhibit strong luminescence in the visible region [11]. Further, it is also quite likely for manganese ions may be linked with phosphate groups, there by strengthening the glass structure and probably increasing the chemical resistance of the glass ceramic.

Manganese ions have strong demeanour on the optical, chemical, magnetic and electrical properties of glasses [12]. So that they have a wide range of applications in various technological fields such as magnetic sensors [13], magneto-optical recording [14] and lasing action [12] etc. Though a reasonably number of recent studies on the environment of manganese ions by means of spectroscopic studies is available but most of them restricted to borate and phosphate glass samples [15–17]. Extension of such studies to glass ceramics is expected to throw more light on structural information and may be useful for increasing the practical applications of these samples. The structural probing of manganese ions, especially in heavy metal oxide-based phosphate glass ceramics is highly desirable since these glass ceramics have potential applications in non-linear optical devices. The present study focuses on the investigations of spectroscopic properties and local structural environment of manganese ions doped calcium zinc bismuth phosphate glass ceramics. The investigated studies include XRD, SEM, DTA, EDS, optical absorption, EPR, FTIR and Raman.

2. Experimental details

In the present investigation glass ceramics with composition $10CaF_2–20ZnO–(15 - x)Bi_2O_3–55P_2O_5:xMnO$ ($0 \leq x \leq 2.5$) were synthesized by melt-quenching and heat treatment method. The prepared samples are labelled as:

$$M0 : 10CaF_2-20ZnO-15.0Bi_2O_3-55P_2O_5$$
$$M5 : 10CaF_2-20ZnO-14.5Bi_2O_3-55P_2O_5 : 0.5MnO$$
$$M10 : 10CaF_2-20ZnO-14.0Bi_2O_3-55P_2O_5 : 1.0MnO$$
$$M15 : 10CaF_2-20ZnO-13.5Bi_2O_3-55P_2O_5 : 1.5MnO$$
$$M20 : 10CaF_2-20ZnO-13.0Bi_2O_3-55P_2O_5 : 2.0MnO$$
$$M25 : 10CaF_2-20ZnO-12.5Bi_2O_3-55P_2O_5 : 2.5MnO$$

The batches of 15 g weight prepared from the proportionate amounts of raw materials of Analytical grade reagents CaF_2 (High media 99.99% pure), ZnO, Bi_2O_3, P_2O_5 and $MnCO_3$ (LOBA, 99.99% pure). The starting materials were weighed using a digital balance (VIBRAHT with an accuracy of ± 0.001 g) carefully and thoroughly mixed in an agate mortar for 40 min then transferred into a 25 ml silica crucible (Infusil make) consequently it is melted at 1300 °C (in air) for 20 min in a PID temperature-controlled furnace until bubble free liquid was formed. All the samples were heat treated in another furnace at their crystalline temperature at 700 °C (which is identified from DTA patterns of the prepared amorphous samples) for 36 h. After then, the samples were allowed to cool slowly to room temperature. The prepared samples were found to be still transparent. The colour of manganese free sample (M0) is in thick brown and the colour of MnO doped samples was observed to change gradually from light brown to grey with an increase of MnO content from 0.5 to 2.5 mol%. The physical appearance of the prepared glass ceramic samples is shown Fig. 1.

The densities and molar volumes of these samples were measured (with an accuracy ± 0.001 g/cm^3) by the standard principle of Archimedes using O-xylene (99.99% pure) as a buoyant liquid with a programmable VIBRA HT density measurement kit. The experimental details of X-ray diffraction (XRD), differential thermal analysis (DTA), Scanning electron microscopy (SEM), Electron paramagnetic resonance (EPR), Optical absorption, Fourier transform infrared (FTIR) and Raman spectral studies of the present glass ceramics are same as that reported in our previous paper [18].

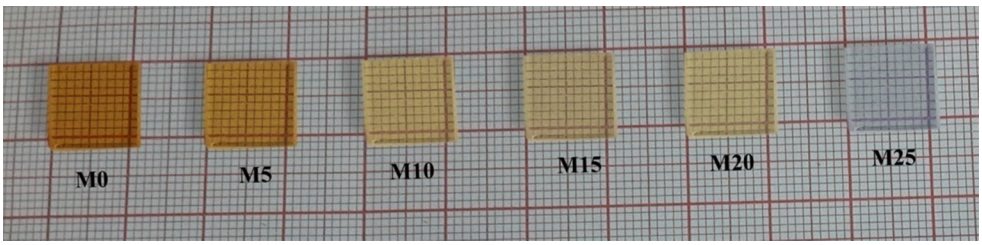

Fig. 1 Photographs of CaF_2–ZnO–Bi_2O_3–P_2O_5: MnO glasses after crystallization

3. Results and discussion

The density (ρ) of manganese undoped glass ceramic sample is found to be 4.020 g/cm^3. The gradual increase in the concentration of nucleating agent MnO in the glass matrix caused a slight decrease in the density. It can be attributed to the partial replacement of high molecular weight (465.96 g/mol) Bi_2O_3 by the low molecular weight (70.94 g/mol) MnO. From the measured values of the density and average molecular weight of the samples, various other physical parameters *viz*., molar volume V_m, manganese ion concentration N_i, mean manganese ion separation R_i, polaron radius R_p of CaF_2–ZnO–Bi_2O_3–P_2O_5: MnO glass ceramics were calculated and presented in Table 1. From this table it has been observed that the density shows an opposite trend to the molar volume for the present glass ceramic samples.

Figure 2 depicts the X-ray diffraction (XRD) patterns of manganese free and doped calcium zinc bismuth phosphate glass ceramics. From these patterns the crystal phases identified based on JCPD data [19] are $Ca_3(PO_4)_2$ (JCPDS NO.070-0364), Bi_3PO_7 (JCPDS NO.044-0645), $CaZn_2(PO_4)_2$ (JCPDS NO.084-1578), $Bi(PO_4)$ (JCPDS NO.089-0287), $Zn_3(PO_4)_2$ (JCPDS NO.076-0604), $Ca(MnF_5)$(JCPDS NO.080-1796), $ZnMn_2O_4$ (JCPDS NO.077-0470), $Mn_2(PO_4)F$ (JCPDS NO.070-1476), MnP_4O_{11} (JCPDS NO.051-0452) and $CaMn(P_2O_7)$ (JCPDS NO.085-1938). Manganese free sample exhibits one major crystalline phase such as bismuth phosphate and three minor crystalline phases *viz*., $Ca_3(PO_4)_2$, $CaZn_2(PO_4)_2$ and $Zn_3(PO_4)_2$ which are kinetically and thermodynamically

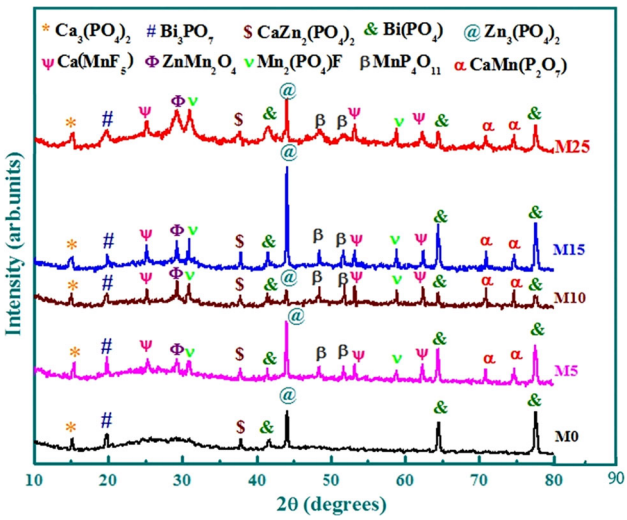

Fig. 2 XRD patterns of CaF_2–ZnO–Bi_2O_3–P_2O_5: MnO glass ceramics

feasible. By the integration of nucleating agent MnO to the host glass system the detected additional crystalline phases *viz*., $Ca(MnF_5)$, $ZnMn_2O_4$, $Mn_2(PO_4)F$, MnP_4O_{11} and $CaMn(P_2O_7)$ are the complexes of either Mn^{3+} or Mn^{2+} ions. The manganese wealthy areas in the glass may enhance its reactivity with the other oxides that precipitate as high density of fine manganese rich crystals. These tiny crystals act as heterogeneous nuclei for the crystallisation for the remaining glass.

Figure 3 shows SEM pictures of the some of the CaF_2–ZnO–Bi_2O_3–P_2O_5: MnO glass ceramic samples. The pictures clearly point out that the samples contain

Table 1 Physical parameters of CaF_2–ZnO–Bi_2O_3–P_2O_5: MnO glass ceramics

Sample	x (mol%)	Density ρ (g/cm^3) (±0.001)	V_m (cm^3/mol) (±0.01)	Manganese ion conc. $N_i \times 10^{21}$ ions/cm^3	Inter ion separation R_i (A^0)	Polaron radius R_p (A^0)
M0	0.0	4.020	42.79	–	–	–
M5	0.5	3.909	43.51	06.922	5.247	2.114
M10	1.0	3.834	43.84	13.738	4.175	1.682
M15	1.5	3.785	43.89	20.585	3.649	1.470
M20	2.0	3.735	43.95	27.410	3.317	1.336
M25	2.5	3.685	44.01	34.216	3.080	1.241

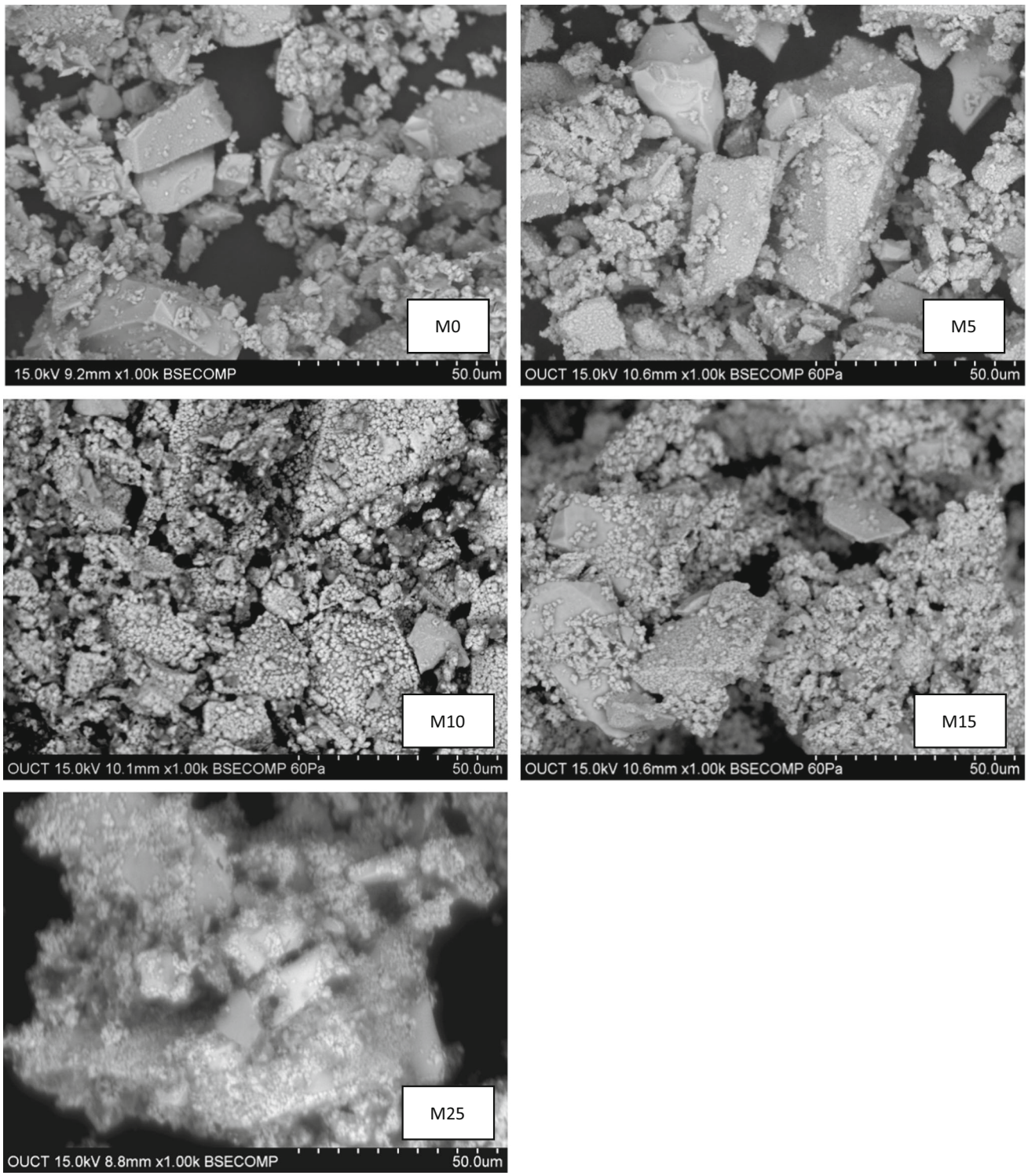

Fig. 3 SEM images of some of the CaF_2–ZnO–Bi_2O_3–P_2O_5: MnO glass ceramics

clear,discrete and arbitrarily distributed crystal grains. The remaining glass phase may act as interconnecting zones among the crystallised areas making the samples free of voids and cracks. The chemical make up of the glass ceramics is characterised by energy dispersive spectrum (EDS) and shown in Fig. 4. This spectrum has indicated that Ca, F, Zn, O, Bi, P and Mn elements are present in various crystalline phases.

Figure 5 shows the differential thermal analysis (DTA) traces of CaF_2–ZnO–Bi_2O_3–P_2O_5: MnO glass ceramics

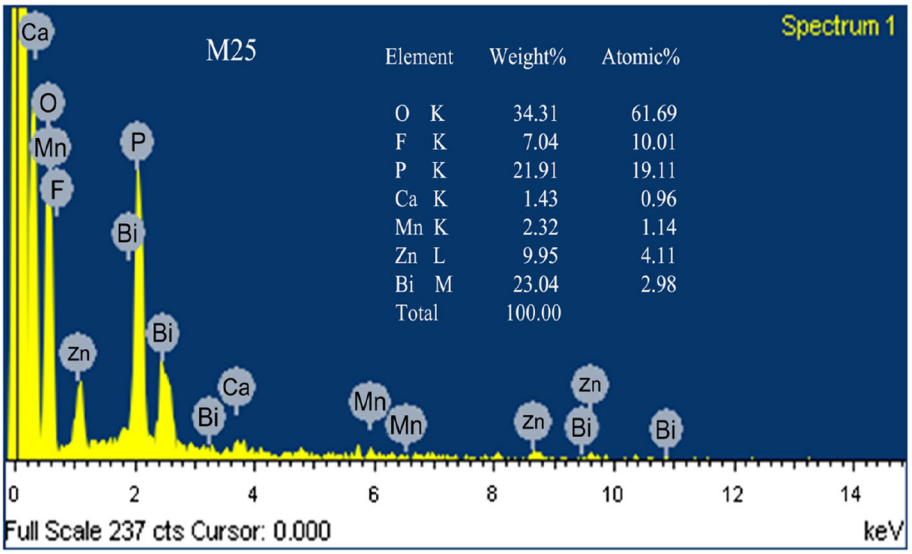

Fig. 4 EDS of $10CaF_2$–$20ZnO$–$12.5Bi_2O_3$–$55P_2O_5$: 2.5MnO glass ceramics

recorded with heating rate of 10 °C per minute. They have exhibited an endothermic peak due to glass transition temperature (T_g) followed by two clear exothermic peaks, Tc_1 and Tc_2 owing to crystallisation and an additional endothermic peak caused by melting (T_m) of the glass ceramics. The observed exothermic peaks refer to the presence of different crystalline phases in the samples. The shape of the crystallization peak in DTA curves signify the variation of enthalpy. The enthalpy of exothermic peaks is observed to increase from 0 to 1 mol% of MnO beyond this it is found to be decreased gradually. The observed increase in enthalpy from M0 to M10 indicates that the crystallization starts initially from the surface of the material and then gradually it is extended to volume of the material. This influence is meagre at higher concentrations of MnO [20]. The SEM pictures of the glass ceramic samples clearly support this view point. The glass transition temperature (T_g) represents the rigidity of the glass

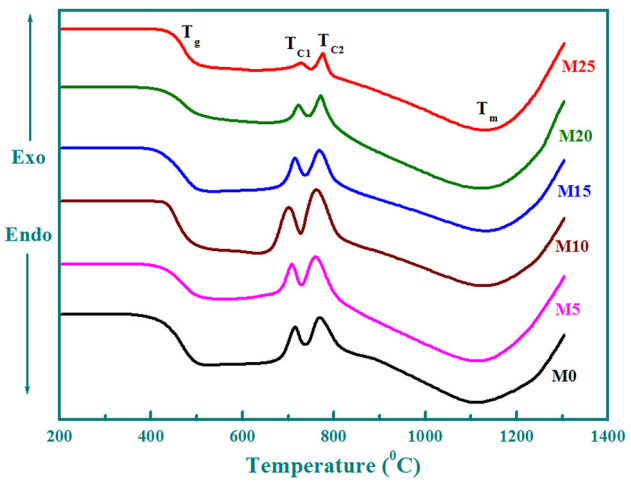

Fig. 5 DTA traces of CaF_2–ZnO–Bi_2O_3–P_2O_5: MnO glass ceramics

ceramic samples and glass forming ability parameter ($Tc_1 - T_g$) related to stability of the glass against devitrification. The observed decrease in T_g and ($Tc_1 - T_g$) values up to 1 mol% of MnO from DTA data indicates that manganese ions could occupy network modifying positions and disrupt the closely packed glass structure (break the oxygen bonding) which in turn increases the number of non-bridging oxygens (NBO's). As a result the depolymerisation of the glass ceramic structure increases. Beyond 1 mol% of MnO the gradual increase in ($Tc_1 - T_g$) indicates the rate of crystallisation decreases and enthalpy value is also found to decrease. Such observation reveals the manganese ions could occupy the network forming positions in the glass ceramic structure at higher concentration of nucleating agent MnO. The data related to DTA are shown in Table 2.

Figure 6 shows the optical absorption spectra of CaF_2–ZnO–Bi_2O_3–P_2O_5: MnO glass ceramics recorded at room temperature. The spectrum of manganese free glass sample has a band around 450 nm and is attributed to $^4S_{3/2} \rightarrow {}^2P_{1/2}$ of Bi^0 particles [21] and this is due to thermal reduction of Bi^{3+} ions into its metallic state. After the addition of nucleating agent MnO to the host glass ceramic system, the

Table 2 Data of DTA patterns of CaF_2–ZnO–Bi_2O_3–P_2O_5: MnO glass ceramics

Sample	T_g (°C)	Tc_1 (°C)	Tc_2 (°C)	$Tc_1 - T_g$ (°C)	T_m (°C)
M0	473	717	765	244	1115
M5	468	710	762	242	1135
M10	463	703	760	240	1140
M15	465	715	770	250	1144
M20	467	722	774	255	1146
M25	470	730	778	260	1150

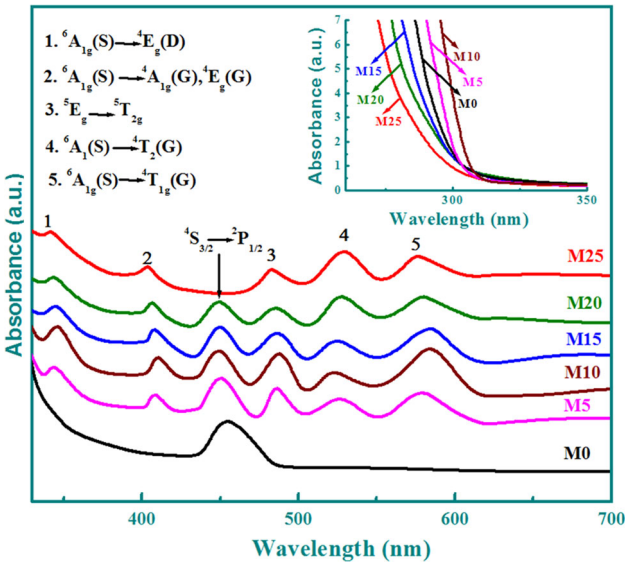

Fig. 6 Optical absorption spectra of CaF_2–ZnO–Bi_2O_3–P_2O_5: MnO glass ceramics. Inset shows absorption edges of all glass ceramics

intensity of this band is observed to decrease slowly up to 2 mol% beyond this it is disappeared. The absorption edge observed at 286 nm for glass ceramic sample M0 and it is found to increase with increase in the concentration of MnO up to1 mol% beyond this concentration the edge exhibited spectrally blue shift. The spectra of manganese doped glass ceramics exhibited two broad bands around 582 and 526 nm as well as two sharp bands at about 408 and 343 nm. The bands around 582, 408 and 343 nm are the octahedral transitions of Mn^{2+} ions and they ascribed respectively to $^6A_{1g}$ (S) → $^4T_{1g}$ (G), $^6A_{1g}$ (S) → $^4A_{1g}$ (G), ^4E_g (G) and $^6A_{1g}$ (S) → ^4E_g (D) transitions. The band at about 526 nm is the tetrahedral transition of Mn^{2+} ions and is assigned as $^6A_1$(S) → $^4T_2$ (G) transition [22, 23]. Besides this, the absorption spectra also consist of a band around 485 nm is due to octahedral transition of Mn^{3+} ions and is ascribed to the transition of ^5E_g → $^5T_{2g}$ [24]. With increase in the concentration of crystallizing agent MnO up to 1 mol%, the octahedral bands are observed to grow at the expense of the tetrahedral bands with minor red shift in the peak position where as beyond 1 mol% reverse trend is noticed. The octahedrally positioned manganese ions similar to the zinc ions, depolymerize the glass ceramic network by creating more bonding defects and non-bridging oxygens in the samples doped with MnO up to 1 mol%. Optical band gap energy (E_g) is estimated for all these glass ceramic samples from Tauc's plot curves, drawn between $(\alpha h\upsilon)^{1/2}$*vs* photon energy (*hυ*), extrapolated to the X-axis where $(\alpha h\upsilon)^{1/2} = 0$ are shown in Fig. 7. The value of optical band gap (E_g) with the concentration of MnO exhibited minimal effect at x = 1 mol% (M10 sample) and found to increase for further increase of nucleating agent MnO. In other words the observed decrease in the optical acivation energy associated with octahedral bands of Mn^{2+} ions with an increase of nucleating agent MnO up to 1 mol% (Table 3) is a clear confirmation concerning intervalence transfer or polaronic type of absorption between Mn^{2+} and Mn^{3+} species [11]. Urbach plots drawn between *ln(α) vs* photon energy (*hυ*) for the investigated glass ceramic samples are shown in Fig. 8. The values of Urbach energy (ΔE) were calculated by determining the reciprocals of slopes of the linear region of the curves. The value of Urbach energy (ΔE) is found to be maximum 0.418 eV for M10 sample (i.e.1 mol% of MnO doped glass) and decreases for further increase in the concentration of MnO. The data related to optical absorption spectral studies are presented in Table 3. Figure 9 represents Tanabe-Sugano diagram for octahedrally coordinated Mn^{2+} ions. Using this diagram the crystal field splitting parameter (Dq), Racah parameters (B and C) and nephelauxetic ratio β ($B_{complex}/B_{free\ ion}$) are calculated and these are presented in Table 4. The calculated values of Dq, B and C are in good agreement with the values reported in literature for Mn^{2+} ions in an octahedral symmetry [25]. Figgis [26] reported that 960 cm^{-1} is the value for Racah parameter of Mn^{2+} free ion ($B_{free\ ion}$).

Mn^{2+} ions belong to d^5 configuration. The ground state of the d^5 system in a weak octahedral crystal field has one electron in each d orbital, and their spins are parallel, making it a spin sextuplet. This corresponds to the ^6S ground state of the free ion, which is not split by the ligand field. However, this is the only sextuplet state possible, for every conceivable alteration of the electron distribution $(t_{2g})^3(e_g)^2$ results in pairing of two or four spins, thus making quartet or doublet states. Hence, all excited states of d^5 system have different spin multiplicity from the ground state, and these transitions are spin forbidden. Because of weak spin–orbit interactions, such transitions

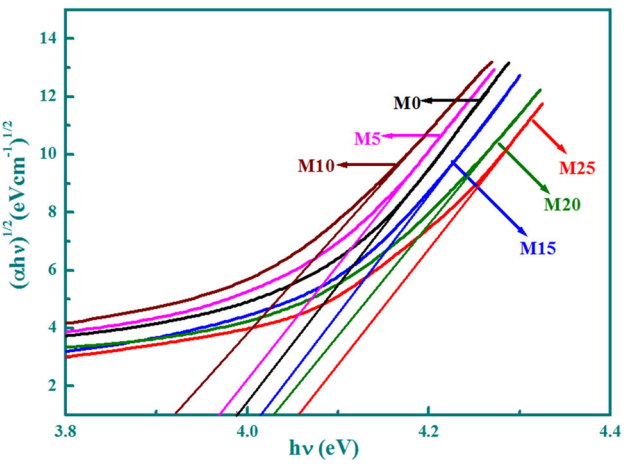

Fig. 7 Tauc's plots of CaF_2–ZnO–Bi_2O_3–P_2O_5: MnO glass ceramics

Table 3 Data on optical absorption spectra of CaF_2–ZnO–Bi_2O_3–P_2O_5: MnO glass ceramics

Assignment	M0	M5	M10	M15	M20	M25
Absorption edge λ_c (nm)	286	290	295	282	277	272
Optical band gap E_g (eV) (±0.01)	3.99	3.97	3.92	4.01	4.03	4.06
Urbach's Energy ΔE (eV) (±0.001)	0.310	0.371	0.418	0.307	0.276	0.259
Band positions of O_h transitions of Mn^{2+} ions (nm)						
$^6A_{1g}$ (S) → $^4T_{1g}$(G)	–	582	587	583	580	576
$^6A_{1g}$ (S) → $^4A_{1g}$(G),^4E_g(G)	–	408	410	407	406	403
$^6A_{1g}$ (S) → ^4E_g(D)	–	343	347	345	343	341
Band Positions of T_d transitions of Mn^{2+} ions (nm)						
$^6A_1$ (S) → $^4T_2$(G)	–	526	523	525	527	529
Band Positions of O_h transitions of Mn^{3+} ions (nm)						
^5E_g → $^5T_{2g}$	–	485	488	486	484	482

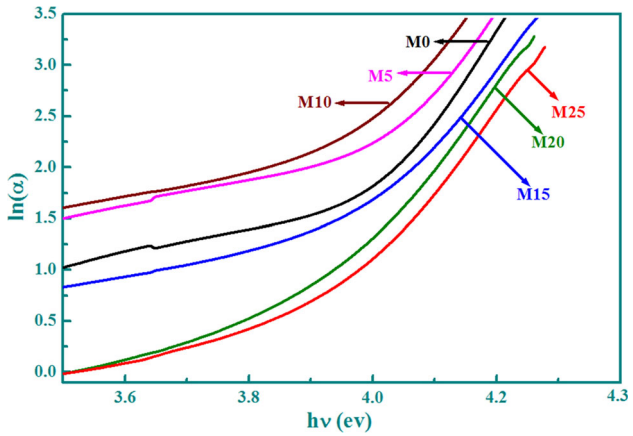

Fig. 8 Urbach plots of CaF_2–ZnO–Bi_2O_3–P_2O_5: MnO glass ceramics

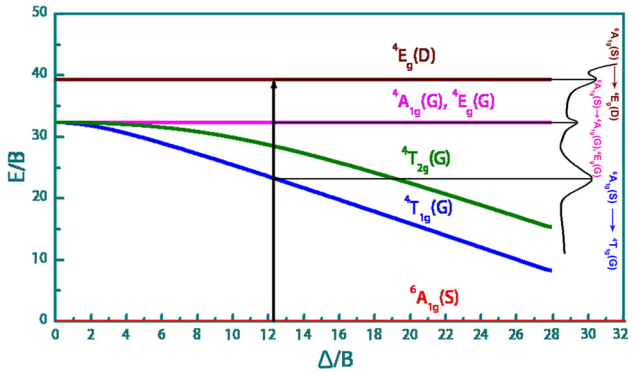

Fig. 9 Tanabe-Sugano diagram for octahedrally coordinated Mn^{2+} ions and corresponding optical absorption spectrum for glass ceramic sample M10

are not totally absent, but they give rise only to very weak absorption bands. The splittings in a tetrahedral crystal field are identical to those in an octahedral crystal field in d^5 system. In the octahedral crystal field the free ion terms ^6S transform as $^6A_{1g}$, ^4P transform as $^4T_{1g}$, ^4D splits into $^4E_g + {}^4T_{2g}$ and ^4G splits into $^4A_{1g} + {}^4E_g + {}^4T_{2g} + {}^4T_{1g}$ respectively. $^6A_{1g}$ lies lowest according to Hunds' rule [24, 27]. From the absorption spectra (Fig. 6) the observed bands due to $^6A_{1g}$ (S) → $^4A_{1g}$ (G), ^4E_g (G) and $^6A_{1g}$ (S) → ^4E_g (D) are sharp as they arise from intra configurational transitions. The transitions $^6A_{1g}$(S) → $^4T_{1g}$ (G) and $^6A_1$(S) → $^4T_2$ (G) involve a change of configuration from $(t_{2g})^3(e_g)^2$ to $(t_{2g})^4(e_g)^1$ and $(e)^2(t_2)^3$ to $(e)^3(t_2)^2$ are observed to be broad. The band at about 485 nm is assigned to spin allowed transition ^5E_g → $^5T_{2g}$ suggests that a part of manganese ions exists in Mn^{3+} (d^4 electronic configuration) and occupy octahedral positions in the glass ceramics [24, 28]. This band arises due to the intra configurational transition between the two Jahn–Teller split quintet levels, *viz*., the ^5E ground state and the $^5T_2$ excited state. The gradual increment in the concentration of octahedrally positioned manganese ions up to 1 mol% of nucleating agent MnO, causes a formation of large number of donor centres and consequently, the excited states of localised electrons originally fascinated on Mn^{2+} sites begin to overlap with the empty 3d states on the neighbouring impurity sites. Thus, the impurity band becomes more extended into the main band gap. This might have shifted the absorption edge towards higher wavelength which causes a considerable contraction in the band gap as observed. So that octahedrally coordinated manganese ions act as network modifiers. Similarly, the concentration of nucleating agent MnO is increased above 1 mol%, the intensity of tetrahedral band grows at the expense of octahedral band with red shift. As a result majority of Mn^{2+} ions occupy network-forming position which causes the decrease in the concentration of non-bridging oxygens in the glass matrix. This leads to decrease in the degree of localisation of electrons, thereby a decrease in the donor centres is expected. The decrease of these centres leads to increase of E_g and shifts the absorption edge towards lower wavelength side. The observed blue-shift of E_g is

Table 4 Crystal field splitting and Racah parameters of CaF_2–ZnO–Bi_2O_3–P_2O_5: MnO glass ceramics

Sample	Crystal field splitting parameter Dq (cm^{-1})	Racah parameters		Nephelauxetic ratio β
		B (cm^{-1})	C (cm^{-1})	
M5	908.48	738	3304	0.769
M10	898.63	730	3268	0.760
M15	904.79	735	3291	0.766
M20	909.71	739	3309	0.770
M25	914.63	743	3326	0.774

associated with increase in the exchange interactions between the p-electrons in the conduction band of P_2O_5 and the localized d-electrons of the substitutionally (tetrahedrally) positioned manganese ions. The variation of Urbach energy with concentration of MnO also supports the above view point.

Crystal field splitting parameter (Dq) describes splitting of d-level in the cubic crystal field while Racah parameters (B & C) explain Coulomb and exchange interactions in the d shell. The values of Dq, B and C are calculated from the Tanabe-Sugano diagram of octahedrally coordinated Mn^{2+} ions using three octahedral transitions. If the value of Dq/B $\ll$ 2.8, then Mn^{2+} ions lie in the weak crystal field environment or if the value of Dq/B $\gg$ 2.8, then Mn^{2+} ions recline in the strong crystal field environment or if the value of Dq/B = 2.8, then Mn^{2+} ions exist in the intermediate crystal field environment [10]. In the present case the value of Dq/B = 1.23, which implies that Mn^{2+} ions lie in the weak crystal field environment. With the help of the Racah parameter B, the nephelauxetic ratio (β) has also been evaluated (Table 4). This ratio (β) gives the information about the delocalization of electrons from the metal ions into molecular orbital covering both metals and ligands. The lower value of β(nephelauxetic ratio) for glass M10 indicates the maximum delocalization effect in the sample and this value increases gradually from M10 to M25 samples and attains the highest value for M25 sample indicating the lower is the delocalization effect. Hence, the rigidity of the glass ceramic network increases from M10 to M25 sample.

EPR of Mn^{2+} ions may provide useful information regarding the structural details of the vitreous matrix shown by their distribution on different structural units building the network, their coordination and the valence states. In order to investigate the coordination environment of the manganese ions in the present glass ceramics an EPR analysis was performed. Figure 10 represents the typical EPR spectra of CaF_2–ZnO–Bi_2O_3–P_2O_5 glass ceramics doped with different concentrations of MnO observed at room temperature. The EPR spectra of the samples doped with MnO have exhibited a resonance signal around g_2 = 2.023 with a six line hyperfine structure(hfs) and

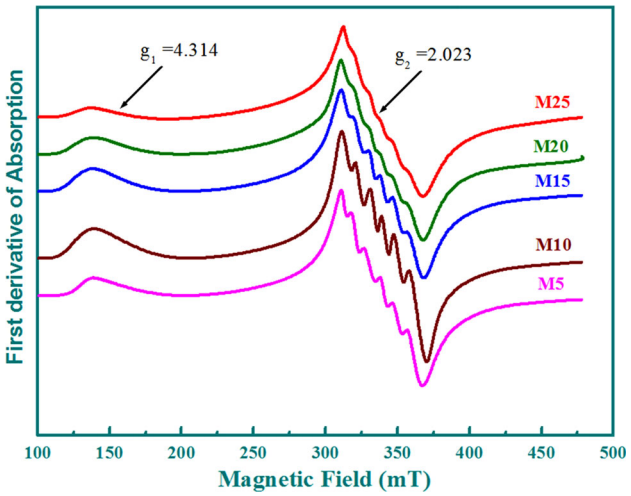

Fig. 10 EPR spectra of CaF_2–ZnO–Bi_2O_3–P_2O_5: MnO glass ceramics

another signal at about g_1 = 4.314. The relative intensity and half-width of these two signals are observed to increase with the increase in the concentration of manganese ions up to 1 mol% beyond this concentration it is found to decrease gradually. The values of g_1, g_2 and hyperfine splitting parameter (A) of Mn^{2+} ions for the present glass ceramics are calculated and presented in Table 5. These values are compared with that of other glass system [22] and found in good agreement.

$^6S_{5/2}$ is its free ion ground state and possesses zero total orbital angular momentum. Hence an EPR signal is expected with 'g' value very close to the free electron value g_{eff} = 2.0023. Since the total orbital angular momentum is zero, in the first order there can be no interaction with the crystal field and any higher order interactions must arise from fine structure terms. The axial distortion of octahedral symmetry gives rise to three Kramer's doublets ($m_s = \pm 5/2$, $m_s = \pm 3/2$, and $m_s = \pm 1/2$). Application of Zeeman field splits the spin degeneracy of these Kramer's doublets. As the crystal field splitting is normally much greater than the Zeeman field, the resonance signals observed are due to transitions within the Kramer's doublets split by the Zeeman field [29]. In the present study, the observed resonance signal around

Table 5 Summary on EPR spectra of CaF_2–ZnO–Bi_2O_3–P_2O_5: MnO glass ceramics

Sample	x (mol%)	g_1 (±0.001)	g_2 (±0.001)	hfs parameter A (mT)
M5	0.5	4.293	1.997	9.470
M10	1.0	4.282	1.991	9.715
M15	1.5	4.301	2.007	9.613
M20	2.0	4.309	2.020	9.515
M25	2.5	4.314	2.023	9.475

$g_2 = 2.023$ at higher field is given by two enclosed signals: one signal with resolved hyperfine structure (given by the isolated Mn^{2+} ions) and another signal comes from the Mn^{2+} ions involved in dipole–dipole type interactions. This resonance signal is also due to Mn^{2+} ions which are in an environment close to octahedral symmetry and is arisen from the transition between the energy levels of the lower doublet ($m_s = \pm 1/2$). While the other resonance signal around $g_1 = 4.314$ at lower field is the characteristic of isolated Mn^{2+} ions predominantly situated in tetragonally and/or rhombically distorted octahedral sites of symmetry subjected to strong crystal field effects and is due to the transition between the energy levels of the middle doublet ($m_s = \pm 3/2$). In the present glass ceramics the intensity of the resonance signal at about $g_1 = 4.314$ is much lower than at $g_2 = 2.023$. This may be due to the number of Mn^{2+} ions present in rhombic surroundings is low compared to those in octahedral positions. The ability to observe the ^{55}Mn hyperfine structure has two concrete benefits, i) it generally allows clear-cut assignments of positions of complex resonance lines to manganese and ii) the magnitude of hyperfine splitting constant provides a measure of the bonding between Mn^{2+} ions and its surrounding ligands. The six-line hyperfine structure at about $g_2 = 2.023$ is analysed using the equation [30]

$$H_m = H_0 - A \cdot m_I - A^2\left[\left(35 - 4m_I^2\right)/8H_0\right] \quad (1)$$

where $H_0 = h\nu/g_0\beta$, $m_I = -5/2, -3/2, -1/2, 1/2, 3/2, 5/2$, g_0 is the isotropic g factor and A is the hyperfine splitting constant. Van Wieringen [31] noted that the strength of the hyperfine splitting depends on the matrix into which the ion is dissolved and is mainly determined by the electro negativity of the neighbours. This means a qualitative measure of the covalency of the bonding in the matrix can be determined from the value of hyperfine splitting constant A. Lower the value of A, the more covalent bonding of the anion in the glass ceramic matrix. The magnitude of the hyperfine splitting constant A can be measured using the expression [32]:

$$A = \left[\left(\Delta_{Opp} + \Delta_{Ott}\right)/5 + \left(\Delta_{Mpp} + \Delta_{Mtt}\right)/3 + \left(\Delta_{Ipp} + \Delta_{Itt}\right)\right]/6 \quad (2)$$

where Δ_{Opp} and Δ_{Ott} represent the differences between the first and sixth peak positions, measured peak to peak and trough to trough respectively. Δ_{Mpp} and Δ_{Mtt} represent difference in positions between second and fifth peaks, Δ_{Ipp} and Δ_{Itt} between second and third peaks.

In the present work, the evaluated hyperfine splitting(hfs) constant A (Table 5) is found to increase up to 1 mol% of MnO indicates that the increase of ionic nature of the bonding between Mn^{2+} ions and the neighbouring ligands and beyond this concentration covalency around Mn^{2+} ions increases. The intensity and line width around $g_2 = 2.023$ resonance signal are found to increase gradually with an increase in the content of MnO up to 1 mol%. Which indicates the Mn^{2+} ions that might be responsible for the broadening of EPR lines participated in dipolar interaction. The increasing ionic bonding nature between Mn^{2+} ions and O^{2-} ions generating the octahedral symmetric ligand field was evidenced from the rise of hfs constant (A) with the content of MnO. It is also noted that the g value for the hyperfine splitting is an indicative of the nature of bonding in the glass. If the g value shows a negative shift with respect to $g_{eff} = 2.0023$, then the bonding is ionic and conversely if the shift is positive then the bonding is more covalent in nature. Therefore in the present work the observed negative shift in the g-value increases up to 1 mol% of nucleating agent MnO represents that Mn^{2+} ions are in an ionic environment and occupy octahedral positions whereas the increase in positive shift in the g value beyond 1 mol% of MnO indicates the more covalence nature and occupy tetrahedral positions in the glass ceramic matrix.

In general, the intensity of signal is proportional to the number of EPR active species involved in the resonance absorption. The non-linear variation in the intensity of the resonance lines with manganese concentration shows that the manganese ions in glass ceramics are present in both Mn^{2+} and Mn^{3+} states. The existence of the two valence states for manganese ions in glass ceramics is due to the synthesis procedure or the spin–spin interactions. The presence of Mn^{3+} ions has been confirmed by optical absorption and XRD studies.

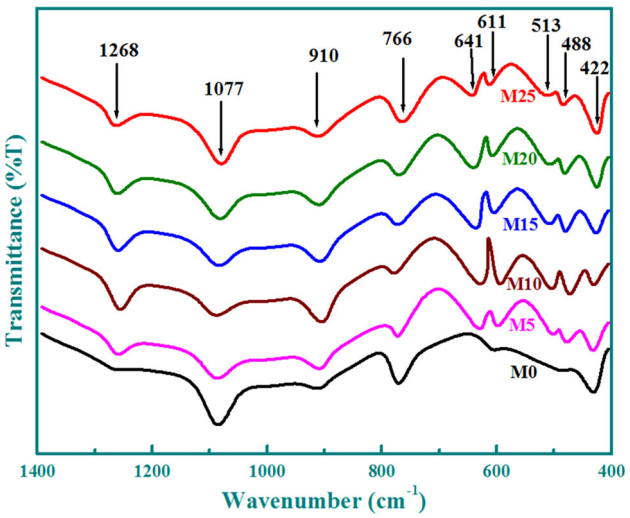

Fig. 11 FTIR spectra of CaF_2–ZnO–Bi_2O_3–P_2O_5: MnO glass ceramics

The infrared spectrum is the unique characteristic of functional groups comprising the molecule and is found to be the most useful physical method of investigation in identifying functional groups and to know the molecular structure. The FTIR data show that the controlled addition of MnO in the structure of analysed glass ceramics generates several rearrangements in the network structure at the short-range order level. The infrared transmission spectra of CaF_2–ZnO–Bi_2O_3–P_2O_5: MnO glass ceramics recorded in the wavenumber range 1400–400 cm^{-1} are shown in Fig. 11. The identified vibrational modes and their corresponding assignments are presented in Table 6. The vibrational bands at about 1268 cm^{-1} attributed to P = O stretching vibration/anti-symmetrical vibrations of PO_2^- groups, 1077 cm^{-1} due to symmetric stretching vibrations of Q^2 (PO_2) groups, 910 cm^{-1} due to P–O–P asymmetric stretching vibrations, 766 cm^{-1} due to P–O–P symmetrical stretching vibrations, 488 cm^{-1} due to O–P–O bending vibrations [33, 34] are noticed. The band due to Bi–O vibrations of distorted BiO_6 units is at about 611 cm^{-1} [35]. Another band is observed at about 422 cm^{-1} is ascribed to ZnO_4 structural units [8]. With the introduction of MnO (from 0.5 to 2.5 mol%) into the glass network, two new vibrational bands are noticed around 513 and 641 cm^{-1} are due to specific vibrations of Mn–O bonds [36]. With the gradual addition of MnO up to 1 mol%, a progressive increase in the intensity (with a shift towards slightly lower wavenumber) of the bands due to PO_2^- asymmetric groups/P = O stretching vibrations, P–O–P asymmetric stretching vibrations, Bi–O vibrations of distorted BiO_6 units, O–P–O bending vibrations and specific vibrations of Mn–O bonds has been observed. Whereas the bands corresponding to ZnO_4 units, P–O–P symmetric stretching vibrations and symmetric stretching vibrations of $(PO_2)^-$ groups are shifted towards higher wavenumber with a considerable decrease in the intensity. With the increase of the concentration of nucleating agent MnO above 1 mol%, the reverse trend is observed. The ionic radius (0.080 nm) of Mn^{2+} ion is close to that (0.074 nm) of Zn^{2+} ion and their valencies are equal. So that there is a possibility for Mn^{2+} ions can occupy Zn^{2+} ion sites in these glass ceramics [37]. As a result the intensity of ZnO_4 structural units is found to decrease with the increase of Mn–O specific vibrations. From the obtained spectra it follows that the increasing content of MnO up to 1 mol% in the structure of calcium zinc bismuth phosphate glass ceramics causes the breaking the existing linkages, i.e. Bi–O–Bi, Bi–O–P and P–O–P and the formation of cross linkages of Bi–O–Mn and/or P–O–Mn takes place. It is responsible for the increase in the degree of depolymerisation of the present glass ceramics up to 1 mol% of MnO. It means that both Mn^{2+} and Mn^{3+} ions act as network modifier. Therefore, the gradual increase in the intensity of symmetrical vibrational bands beyond 1 mol% of MnO in the IR spectra indicates the increase of tetrahedrally coordinated Mn^{2+} ions which in turn increases the polymerisation in the glass ceramic matrix due to network forming action of these ions. Structural model for manganese ions occupying tetrahedral

Table 6 Data on FTIR spectra of CaF_2–ZnO–Bi_2O_3–P_2O_5: MnO glass ceramics (band positions are in cm^{-1})

M0	M5	M10	M15	M20	M25	Assignment
427	430	435	427	425	422	Vibrations of ZnO_4 units
482	480	475	482	485	488	O–P–O bending vibrations
–	500	497	506	509	513	Specific vibrations of Mn–O bonds
604	599	596	605	608	611	Bi–O vibrations of distorted BiO_6 units
–	630	626	634	638	641	Specific vibrations of Mn–O bonds
774	777	780	774	770	766	P–O–P symmetric vibrations
907	905	901	905	908	910	P–O–P asymmetric stretching vibrations
1085	1088	1091	1083	1080	1077	Symmetric stretching vibrations of Q^2 (PO_2) groups
1265	1262	1256	1263	1265	1268	PO_2^- asymmetric groups/P = O stretching vibrations

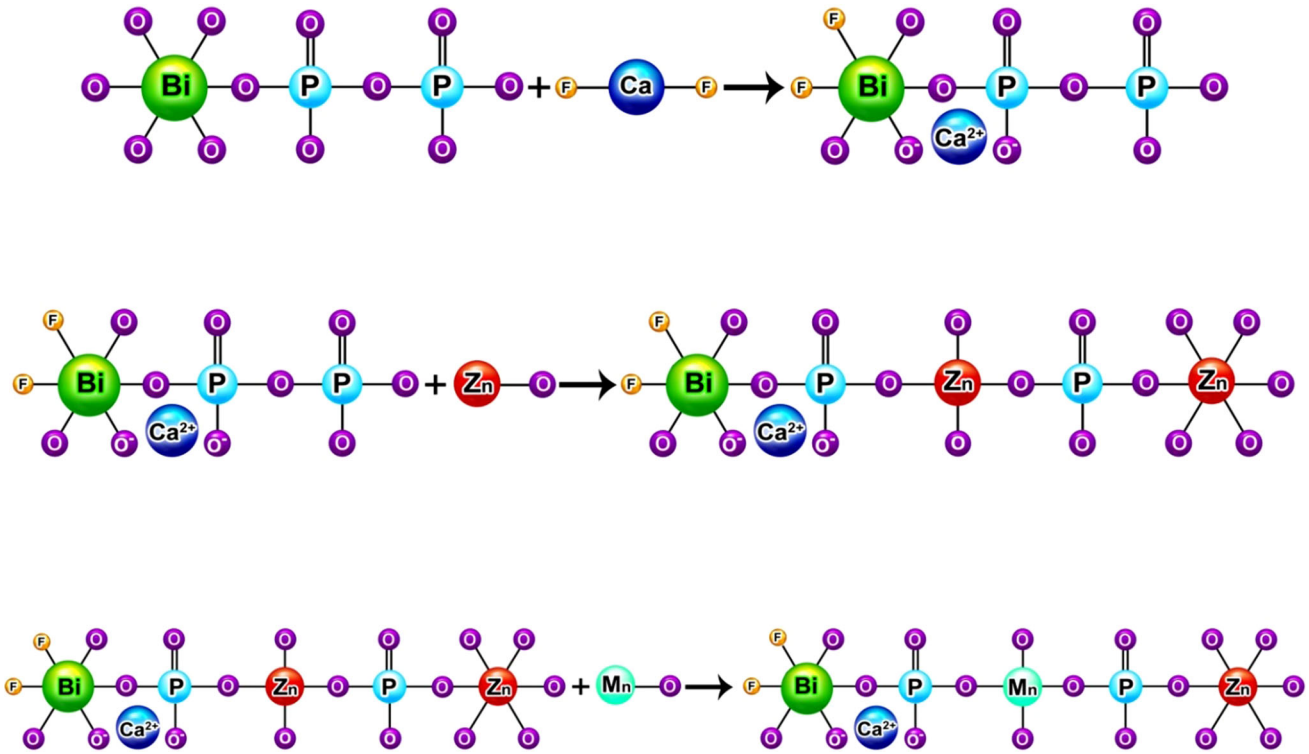

Fig. 12 Schematic illustration for structural arrangement of CaF_2–ZnO–Bi_2O_3–P_2O_5: MnO glass ceramic matrix

positions in calcium zinc bismuth phosphate glass ceramics is shown in Fig. 12.

Figure 13 shows the Raman spectra of all titled glass ceramic samples. The corresponding assignments of these bands are furnished in Table 7. The spectrum of manganese free sample has exhibited main conventional bands due to phosphate groups:

(i) around 1274 and 1124 cm^{-1} are due to asymmetric PO_2^- stretching mode and symmetric stretching modes of non-bridging atoms on Q^2 tetrahedra of (PO_2) respectively [38],

(ii) around 1023 and 966 cm^{-1} are due to PO_2 symmetric mode (Q^1) [39] and $P-O^-$ symmetric stretching vibrations of PO_4^{3-} units [40], (iii) around 658 cm^{-1} is due to symmetric vibrations of P–O–P in Q^2 units respectively and (iv) 418 cm^{-1} is due to bending vibrations of PO_4 units [39]. The Bi–O and Bi–O–Bi vibrations of distorted BiO_6 units are observed around 584 and 368 cm^{-1} respectively and the band around 269 cm^{-1} assigned to Bi–O breathing vibrations of BiO_3 pyramidal units are also noticed in these spectra [41]. The band around 444 cm^{-1} is due to ZnO_4 structural units and the band at 224 cm^{-1} is ascribed to ZnO_6 units [42]. With the integration of MnO to the glass ceramic samples, the Raman spectra clearly shows a well resolved new band located at about 747 cm^{-1} and is attributed to symmetric stretching vibrations of MnO_4 tetrahedra [43]. The spectra show that with increase in the concentration of nucleating agent MnO all the asymmetrical vibrational bands are observed to grow at the expense of the symmetrical bands up to 1 mol% beyond that symmetrical vibrational bands grow at the expense of the asymmetrical bands.

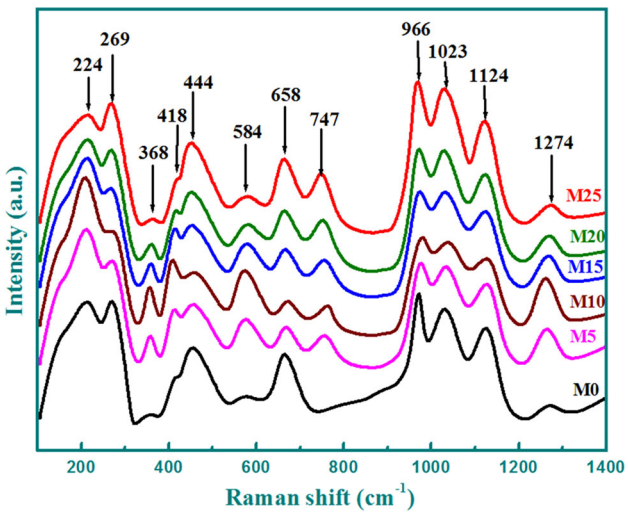

Fig. 13 Raman spectra of CaF_2–ZnO–Bi_2O_3–P_2O_5: MnO glass ceramics

Thus the analysis of FTIR and Raman spectra of the samples has revealed that the rigidity of the glass ceramic

Table 7 Data on Raman spectra of CaF_2–ZnO–Bi_2O_3–P_2O_5: MnO glass ceramics (band positions are in cm^{-1})

M0	M5	M10	M15	M20	M25	Assignment
219	215	210	218	221	224	ZnO_6 units
273	277	282	274	272	269	BiO_3 pyramidal units
361	358	356	361	364	368	Bi–O–Bi stretching vibrations in distorted BiO_6 units
413	409	404	412	415	418	Bending vibrations of PO_4 units
450	454	458	449	446	444	ZnO_4 units
578	574	570	578	581	584	Bi–O vibrations in distorted BiO_6 units
661	665	669	663	660	658	P–O–P symmetric mode Q^2
–	756	761	752	750	747	Symmetric stretching vibrations of MnO_4 tetrahedral units
973	976	981	972	969	966	$P-O^-$ symmetric stretching vibrations of PO_4^{3-} units
1028	1032	1037	1029	1026	1023	PO_2 symmetric mode (Q^1)
1129	1133	1136	1129	1127	1124	PO_2 symmetric mode (Q^2)
1267	1263	1259	1268	1270	1274	Asymmetric (PO_2^-) stretching mode

structure is observed to decrease due to increase of non-bridging oxygens and depolymerises the network up to 1 mol% of MnO beyond this concentration the strength of the glass ceramics is found to increase. The same inference was also drawn from the analysis of optical absorption and EPR spectra of the titled glass ceramics.

4. Conclusions

CaF_2–ZnO–Bi_2O_3–P_2O_5 glasses doped with different concentrations of nucleating agent MnO (ranging from 0 to 2.5 mol%) were crystallised by heat treatment. The prepared glass ceramics were characterized by XRD, DTA, SEM, EDS, optical absorption, EPR, FTIR and Raman studies. The XRD patterns of ceramic samples have exhibited various crystal phases *viz*., $Ca_3(PO_4)_2$, Bi_3PO_7, $CaZn_2(PO_4)_2$, $Bi(PO_4)$, $Zn_3(PO_4)_2$, $Ca(MnF_5)$, $ZnMn_2O_4$, $Mn_2(PO_4)F$, MnP_4O_{11} and $CaMn(P_2O_7)$. The optical absorption spectra studies of the samples have revealed the existance of manganese ions in Mn^{3+} state in addition to Mn^{2+} state. From the optical absorption data the crystal field parameters Dq, B and C are evaluated using octahedral transitions of Mn^{2+} ions. The observed value of Dq/B = 1.23, indicated that Mn^{2+} lies in weak crystal field environment. EPR spectral studies have indicated that Mn^{2+} ions occupy predominantly octahedral positions in the glass ceramic matrix of the samples doped with lower content of MnO. These studies have also indicated the bonding of manganese ions with ligands is mostly covalent in nature especially in the samples with higher content of nucleating agent MnO. FTIR and Raman studies have revealed that the degree of disorder in the glass ceramic net work increases with increase in the concentration of MnO up to 1.0 mol% beyond this concentration it is observed to decrease and it enhances the rigidity of the glass ceramic structure. Therefore, from the analysis of these investigations it is concluded that the samples doped with higher concentration of MnO are suitable for insulating devices.

Acknowledgements The authors are thankful to the University Grants Commission (UGC) and the Department of Science and Technology (DST), New Delhi, India for sanctioning DSA and FIST level-I projects respectively to the Physics Department of the University.

References

[1] W Höland and G H Beall *Glass-Ceramic Technology*, 2nd edn. (New Jersey: The American Ceramic Society, John Wiley & Sons, Inc.) p 1 (2012)
[2] X Duan, D Yuan, X Cheng, Z Liu and X Zhang *J. Alloys Compd.* **453** 379 (2008)
[3] J H Campbell and T I Suratwala *J. Non-Cryst. Solids* **263&264** 318 (2000)
[4] L L Hench *J. Am. Ceram. Soc.* **74** 1487 (1991)
[5] M H Wan, P S Wong, R Hussin, H O Lintang and S Endud *J. Alloys Compd.* **595** 39 (2014)
[6] S Rani, S Sanghi, A Agarwal and N Ahlawat *J. Alloys Compd.* **477** 504 (2009)
[7] M A Marzouk, F H ElBatal, K M ElBadry and H A ElBatal Spectrochim. Acta Part A **171** 454 (2017)
[8] P Srinivasa Rao, P M Vinaya Teja, A Ramesh Babu, Ch Rajyasree and D Krishna Rao. *J. Non- Cryst. Solids* **358** 3372 (2012)
[9] A G Dias, J M S Skakle, I R Gibson, M A Lopes and J D Santos *J. Non- Cryst. Solids* **351** 810 (2005)
[10] C Parthasaradhi Reddy, V Naresh and K T Ramakrishna Reddy *Opt. Mater.* **51** 154 (2016)
[11] A V Ravi Kumar, Ch Srinivasa Rao, N Narasimha Rao, V Ravi Kumar, I V Kityk and N Veeraiah. *J. Non- Cryst Solids* **358** 1278 (2012)
[12] M Srinivasa Reddy, G Murali Krishna and N Veeraiah *J. Phys. Chem. Solids* **67** 789 (2006)
[13] V S Raghuwanshi et al. *J. Non-Cryst. Solids* **385** 24 (2014)

[14] A Winterstein, H Akamatsu, D Moncke, K Tanaka, M A Schimidt and L Wondraczek *Opt. Mater. Express* **3** 184 (2013)
[15] P Pascuta, M Bosca, G Borodi and E Culea *J. Alloys Compd.* **509** 4314 (2011)
[16] J Holubova, Z Cernosek, E Cernoskova and L Benes *J. Therm. Anal. Calorim.* **122(1)** 47 (2015)
[17] S Yusub, P Srinivasa Rao and D Krishna Rao *J. Alloys Compd.* **663** 708 (2016)
[18] A Suneel Kumar, T Narendrudu, S Suresh, M V Sambasiva Rao, G Chinna Ram and D Krishna Rao *J. Non- Cryst. Solids* **434** 62 (2016)
[19] JCPDS-International Centre for Diffraction Data *Powder Diffraction File alphabetical index Inorganic Compounds* (USA: JCPDS, International Centre for Diffraction Data, Newtown Square, PA) (2003)
[20] F Branda, A Buri, A Marotta and S Saiello *Thermochim. Acta* **77** 13 (1984)
[21] M Peng, C Zollfrank and L Wondraczek *J. Phys. Condens. Matter* **21** 285106-1 (2009)
[22] A Padmanabham, T Satyanarayana, Y Gandhi and N Veeraiah *Phys. Status Solidi A* **207** 80 (2010)
[23] B Sudhakar Reddy, N O Gopal, K V Narasimhulu, Ch Linga Raju, J L Rao and B C V Reddy *J. Mol. Struct.* **751** 161 (2005)
[24] F A Cotton and G Willkinsin *Advanced Inorganic Chemistry A comprehensive text* (New York: Interscience publishers) (*third ed.)* p 577 (1972)
[25] N Kiran, C R Kesavulu, A Suresh Kumar and J L Rao *Physica B* **406** 3816 (2011)
[26] B N Figgis *Introduction to Ligand Fields* (New Delhi: Wiley Eastern Limited) p 52 (1976)
[27] B Henderson and G F Imbusch *Optical Spectroscopy of Inorganic Solids* (New York: Oxford University Press) p 408 (1989)
[28] C J Ballhausen *Introduction to Ligand Field Theory* (New York: McGraw Hill, Inc.,) (1962)
[29] A Abragam and B Bleaney *Electron Paramagnetic Resonance of Transition Ions* (London: Oxford University Press) edited by W Marshall and D H Wilkinson p 365 (1970)
[30] J L Rao, G L Narendra, B Sreedhar and S V J Lakshman *Phys. Stat. Sol.(b)* **153** 257 (1989)
[31] J S Van Wieringen *Discuss. Faraday Soc.* **19** 118 (1955)
[32] A R Molla, R P S Chakradhar, C R Kesavulu, J L Rao and S K Biswas *J. Alloys Compd.* **512** 105 (2012)
[33] F F Sene, J R Martinelli and L Gomes *J. Non-Cryst. Solids* **348** 30 (2004)
[34] G Little Flower, G Sahaya Baskaran, M Srinivasa Reddy and N Veeraiah *Physica B* **393** 61 (2007)
[35] Y B Saddeek, I S Yahia, K A Aly and W Dobrowolski *Solid State Sci.* **12** 1426 (2010)
[36] I Ardelean, S Cora, R C Lucacel and O Hulpus *Solid State Sci.* **7** 1438 (2005)
[37] N A Lange *Langes Handbook of Chemistry* (Newyork: McGraw-Hill Inc.,) (13th ed.) edited by J A Dean p 3 (1985)
[38] F H El-Batal *Indian J. Pure & Appl. Phys.* **47** 631 (2009)
[39] A M Milankovic, A Santic, V Licina and D E Day *J. Non-Cryst. Solids* **351** 3235 (2005)
[40] D U Tulyaganov, S Agathopouls, J M Ventura, M A Karakassides, O Fabrichnaya and J M F Ferreira. *J. Eur. Ceram. Soc.* **26** 1463 (2006)
[41] P M Vinaya Teja, Ch Rajyasree, S B Murali Krishna, Ch Tirupataiah and D Krishna Rao *Mater. Chem. Phys.* **133** 239 (2012)
[42] S Bala Murali Krishna and D Krishna Rao *J. Alloys Compd.* **509** 7373 (2011)
[43] A Radu, L Baia, W Kiefer and S Simon *Vib Spectrosc.* **39** 127 (2005)